

Molecular Rectification and Conductance Switching in Carbon-Based Molecular Junctions by Structural Rearrangement Accompanying Electron Injection

Richard McCreery,* Jon Dieringer, Ali Osman Solak,[†] Brian Snyder, Aletha M. Nowak, William R. McGovern, and Stacy DuVall

Contribution from the Department of Chemistry, The Ohio State University, Columbus, Ohio 43210

Received May 19, 2003; E-mail: mccreery.2@osu.edu

Abstract: Molecular junctions were fabricated consisting of a 3.7 nm thick layer of nitroazobenzene (NAB) molecules between a pyrolyzed photoresist substrate (PPF) and a titanium top contact which was protected from oxidation by a layer of gold. Raman spectroscopy, XPS, and AFM revealed that the NAB layer was 2–3 molecules thick and was bonded to the two conducting contacts by C–C and N–Ti covalent bonds. The current/voltage behavior of the PPF/NAB(3.7)/Ti junctions showed strong and reproducible rectification, with the current at +2 V exceeding that at –2 V by a factor of 600. The observed current density at +3 V was 0.71 A/cm², or about 10⁵ e[–]/s/molecule. The *i/V* response was strongly dependent on temperature and scan rate, with the rectification ratio decreasing for lower temperature and faster scans. Junction conductivity increased with time over several seconds at room temperature in response to positive voltage pulses, with the rate of increase larger for more positive potentials. Voltage pulses to positive potentials and back to zero volts revealed that electrons are injected from the Ti to the NAB, to the extent of about 0.1–1 e[–]/molecule for a +3 V pulse. These electrons cause an activated transition of the NAB into a more conductive quinoid state, which in turn causes an increase in conductivity. The transition to the quinoid state involves nuclear rearrangement which occurs on a submillisecond to several second time scale, depending on the voltage applied. The quinoid state is stable as long as the applied electric field is present, but reverts back to NAB within several minutes after the field is relaxed. The results are interpreted in terms of a thermally activated, potential dependent electron transfer into the 3.7 nm NAB layer, which brings about a conductivity increase of several orders of magnitude.

Introduction

The electronic properties of several types of molecular junctions have attracted significant interest, because they are fundamental to the growing area of molecular electronics. A metal/molecule/metal junction combines properties of traditional metallic conductors with those of single molecules or groups of molecules, thus raising the prospect of introducing molecular properties into electronic circuits.^{1–14} The mechanism of electron

transport across molecular junctions has been a very active topic of research in part because it involves concepts from electrochemistry, solid-state physics, and long-range electron transfer phenomena in chemical and biochemical systems. Electron tunneling (coherent, incoherent, and resonant), thermally induced hopping, transmission through Schottky barriers, and other processes have been invoked to explain the dependence of current through a molecular junction on applied voltage and temperature.^{15–17} While there is a wide range of behaviors observed for metal/molecule/metal junctions, there is also general agreement that the current/voltage (*i/V*) characteristics are critically dependent on molecular structure and conformation.

The term “molecular junction” is generally reserved for cases where the molecular layer is one or a few monolayers thick, usually in the range of 1–5 nm. Their monolayer or near-

[†] Permanent address: Ankara University, Faculty of Science, Ankara, Turkey.

- (1) Aviram, A.; Ratner, M. *Chem. Phys. Lett.* **1974**, *29*, 277.
- (2) Mujica, V.; Roitberg, A. E.; Ratner, M. A. *J. Phys. Chem.* **2000**, *112*, 6834.
- (3) Mujica, V.; Ratner, M. A. *Chem. Phys.* **2001**, *264*, 365.
- (4) Jortner, J.; Ratner, M. *Molecular Electronics*; Blackwell Science Ltd.: Cambridge, MA, 1997.
- (5) Mirkin, C. A.; Ratner, M. A. *Annu. Rev. Phys. Chem.* **1992**, *43*, 719.
- (6) Datta, S.; Tian, W.; Hong, S.; Reifenberger, R.; Henderson, J. I.; Kubiak, C. P. *Phys. Rev. Lett.* **1997**, *79*, 2530.
- (7) Feldheim, D. L.; Grabar, K. C.; Natan, M. J.; Mallouk, T. E. *J. Am. Chem. Soc.* **1996**, *118*, 7640.
- (8) Brousseau, L. C.; Zhao, Q.; Shultz, D. A.; Feldheim, D. L. *J. Am. Chem. Soc.* **1998**, *120*, 7645.
- (9) Zhou, C.; Deshpande, M. R.; Reed, M. A.; Jones, L.; Tour, J. M. *Appl. Phys. Lett.* **1997**, *71*, 611.
- (10) Tian, W.; Datta, S.; Hong, S.; Reifenberger, R.; Henderson, J. I.; Kubiak, C. P. *J. Chem. Phys.* **1998**, *109*, 2874.
- (11) Kergueris, C.; Bourgoin, J. P.; Palacin, S.; Esteve, D.; Urbina, C.; Magoga, M.; Joachim, C. *Phys. Rev. B* **1999**, *59*, 12505.

- (12) Holmlin, R. E.; Haag, R.; Chabynyc, M. L.; Ismagilov, R. F.; Cohen, A. E.; Terfort, A.; Rampi, M. A.; Whitesides, G. M. *J. Am. Chem. Soc.* **2001**, *123*, 5075.
- (13) Slowinski, K.; Majda, M. *J. Electroanal. Chem.* **2000**, *491*, 139.
- (14) Ranganathan, S.; Steidel, I.; Anariba, F.; McCreery, R. L. *Nano Lett.* **2001**, *1*, 491.
- (15) Rampi, M. A.; Whitesides, G. M. *Chem. Phys.* **2002**, *281*, 373.
- (16) Hong, S.; Reifenberger, R.; Tian, W.; Datta, S.; Henderson, J.; Kubiak, C. P. *Superlattices Microstruct.* **2000**, *28*, 289.
- (17) Chen, J.; Reed, M. A.; Rawlett, A. M.; Tour, J. M. *Science* **1999**, *286*.

monolayer thickness distinguishes molecular junctions from widely studied metal/molecule/metal structures with thick (> 10 nm) molecular films, such as organic light-emitting diodes and classical dielectric capacitors. To date, the vast majority of molecular junctions are based on metal–thiol self-assembled monolayers (SAMs)^{18–22} and Langmuir–Blodgett (L–B) films.^{23–27} Examples include polyphenyl and poly(phenylvinyl) thiol molecules chemisorbed on gold or silver,^{16,28} biphenyl thiols suspended between Au and titanium,²⁹ and L–B structures on Al or Al oxide substrates.^{24,25,27} Molecular junctions constructed with SAM or L–B chemistry have exhibited interesting electronic effects, such as rectification,³⁰ conductance switching,^{20,21,24} and negative differential resistance (NDR).^{17,31,32}

An additional concept relevant to the current report is the injection of charge into a molecular layer, to alter its properties. Examples include redox-mediated electron transfer in redox polymer films,^{33–38} electron injection into conducting polymer films,^{39,40} and electron injection into molecular tunneling junctions.^{41–44} Redox polymer films have exhibited rectification and chemiluminescence, and their behavior has been explained in terms of electron transport between redox centers with or without accompanying motion of ions.^{37,45} The evidence for electron injection into “thick” junctions with 10–100 nm molecular layers is convincing; however, the involvement of electron injection into monolayers in molecular junctions has not yet been established unequivocally. In the case of monolayer

molecular junctions, which exhibit at least some electronic conduction, it is not obvious how to distinguish electron conduction through the junction from a “redox” event which results in stored charge in the monolayer. The former may involve many more electrons than the latter, making a redox event difficult to observe.

The current report investigates the possibility of charge injection in a new type of molecular junction consisting of a graphitic carbon substrate, a covalently bonded monolayer, and a titanium/gold top contact. Nitroazobenzene was bonded covalently to a very flat carbon film by electrochemical reduction of a diazonium reagent. As noted in previous publications, the covalent carbon–carbon bond between the graphitic substrate and organic monolayer is stronger than Au/thiol or L–B bonds; hence more stable junctions might be possible.^{14,46,47} These carbon/molecule/mercury junctions exhibited conductance switching^{14,47} and interesting dependence on temperature,⁴⁶ but the reproducibility of the junction properties limited the conclusions available with a mercury top contact. The Ti contact reported here appears to bond covalently to the top of the monolayer, resulting in covalent bonds at both interfaces of the monolayer with the contacts. Carbon molecule/Ti molecular junctions were investigated primarily to determine the electron transport mechanism(s) through the junction, but, in the process, a potentially valuable phenomenon involving electron injection into the monolayer was revealed.

Experimental Section

Pyrolyzed photoresist films (PPF) were prepared at 1000 °C as described previously,^{48,49} on polished silicon substrates. The Si was boron doped with a resistivity of 1 Ω cm, but the properties of the silicon did not appear to be important. Because the resistivity of the PPF is $\sim 0.005 \Omega$ cm,^{48,49} the PPF carries most of the current and the Si acts merely as a flat, relatively low conductivity substrate. Approximately 2×3 cm samples of Si (1 mm thick) were cut from 4 in. wafers, then spin coated with AZ-P4330-RS positive photoresist (Clariant Corp., Somerville, NJ) until the uncured photoresist thickness was 5–7 μ m. After pyrolysis, the PPF film was approximately 1–2 μ m thick. Pyrolyzed samples were inspected visually for any obvious defects.

Monolayer deposition by reduction of diazonium reagents in acetonitrile is prone to multilayer formation, because electrons may be able to transfer through the initial monolayer to reduce additional diazonium ions.^{14,50,51} Deposition conditions were chosen carefully, and the layer thickness was confirmed with AFM by observing the depth (in tapping mode) of an intentional scratch made in the monolayer with contact mode AFM, as described elsewhere.⁵⁰ Nitroazobenzene (NAB) was chosen for this initial investigation of Ti junctions due to its strong Raman scattering^{52,53} and previous experience with PPF/NAB/Hg junctions.^{14,47} See Supporting Information for additional details on NAB deposition. The NAB film thickness was determined with AFM “scratching”⁵⁰ to be 3.68 ± 0.31 nm, based on 2 independent samples, 3 scratches, and 58 determinations of NAB layer thickness. The rms roughness of the NAB layers was 0.68 nm, slightly greater than the 0.5 nm roughness of the PPF substrate. The length of one NAB molecule is 1.45 nm, so a 3.7 nm layer is 2–3 NAB molecules thick.

- (18) Garcias, D. H.; Tein, J.; Breen, T. L.; Hsu, C.; Whitesides, G. M. *Science* **2000**, *289*, 1170.
- (19) Cygan, M. T.; Dunbar, T. D.; Arnold, J. J.; Bumm, L. A.; Shedlock, N. F.; Burgin, T. P.; Jones, L.; Allara, D. L.; Tour, J. M.; Weiss, P. S. *J. Am. Chem. Soc.* **1998**, *120*, 2721.
- (20) Donhauser, Z. J.; Mantooth, B. A.; Kelly, K. F.; Bumm, L. A.; Monnell, J. D.; Stapleton, J. J.; Price, D. W.; Rawlett, A. M.; Allara, D. L.; Tour, J. M.; Weiss, P. S. *Science* **2001**, *292*, 2303.
- (21) Bumm, L. A.; Arnold, J. J.; Dunbar, T. D.; Allara, D. L.; Weiss, P. S. *J. Phys. Chem.* **1999**, *103*, 8122.
- (22) Slowinski, K.; Chamberlain, R. V.; Miller, C. J.; Majda, M. *J. Am. Chem. Soc.* **1997**, *119*, 11910.
- (23) Collier, C. P.; Wong, E. W.; Belohradsky, M.; Raymo, F. M.; Stoddart, J. F.; Kuekes, P. J.; Williams, R. S.; Heath, J. R. *Science* **1999**, *285*, 391.
- (24) Collier, C. P.; Matternsteig, G.; Wong, E. W.; Luo, Y.; Beverly, K.; Sampaio, J.; Raymo, F. M.; Stoddart, J. F.; Heath, J. R. *Science* **2000**, *289*, 1172.
- (25) Metzger, R. M.; Xu, T.; Peterson, I. R. *J. Phys. Chem. B* **2001**, *105*, 7280.
- (26) Chen, B.; Metzger, R. M. *J. Phys. Chem.* **1999**, *103*, 4447.
- (27) Metzger, R. M.; Chen, B.; Hopfner, U.; Lakshmikantham, M. V.; Vuillaume, D.; Kawai, T.; Wu, X.; Tachibana, H.; Hughes, T. V.; Sakurai, H.; Baldwin, J. W.; Hosch, C.; Cava, M. P.; Brehmer, L.; Ashwell, G. J. *J. Am. Chem. Soc.* **1997**, *119*, 10455.
- (28) Sikes, H. D.; Smalley, J. F.; Dudek, S. P.; Cook, A. R.; Newton, M. D.; Chidsey, C. E. D.; Feldberg, S. W. *Science* **2001**, *291*, 1519.
- (29) Chen, J.; Calvet, L. C.; Reed, M. A.; Carr, D. W.; Grubisha, D. S.; Bennett, D. W. *Chem. Phys. Lett.* **1999**, *313*, 741.
- (30) Scheib, S.; Cava, M. P.; Baldwin, J. W.; Metzger, R. M. *J. Org. Chem.* **1998**, *63*, 3.
- (31) Seminario, J. M.; Zacarias, A. G.; Tour, J. M. *J. Am. Chem. Soc.* **2000**, *122*, 3015.
- (32) Karzazi, Y.; Cornil, J.; Bredas, J. L. *J. Am. Chem. Soc.* **2001**, *123*, 10076.
- (33) Shigehara, K.; Oyama, N.; Anson, F. C. *J. Am. Chem. Soc.* **1981**, *103*, 2552.
- (34) Buttry, D. A.; Anson, F. C. *J. Am. Chem. Soc.* **1983**, *105*, 685.
- (35) Leidner, C. R.; Murray, R. W. *J. Am. Chem. Soc.* **1985**, *107*, 556.
- (36) White, B. A.; Murray, R. W. *J. Am. Chem. Soc.* **1987**, *109*, 2576.
- (37) Terrill, R. H.; Murray, R. W. Electron Hopping Transport in Electrochemically Active, Molecular Mixed Valent Materials. In *Molecular Electronics*; Jortner, J.; Ratner, M., Eds.; Blackwell Science Ltd.: Cambridge, MA, 1997; p 215.
- (38) McCarley, R. L.; Thomas, E. R.; Irene, E. A.; Murray, R. W. *J. Electrochem. Soc.* **1990**, *137*, 1485.
- (39) Epstein, A. J.; Lee, W. P.; Prigodin, V. N. *Synth. Met.* **2001**, *117*, 9.
- (40) Wang, Y. Z.; Epstein, A. J. *Acc. Chem. Res.* **1999**, *32*, 217.
- (41) Mazur, U.; Hipps, K. W. *J. Phys. Chem. B* **1999**, *103*, 9721.
- (42) Hipps, K. W.; Mazur, U. *J. Phys. Chem.* **1994**, *98*, 5824.
- (43) Hipps, K. W.; Mazur, U. Inelastic electron tunneling spectroscopy. In *Handbook of Vibrational Spectroscopy*; John Wiley & Sons Ltd.: Chichester, 2002; Vol. 4, p 812.
- (44) Mazur, U.; Hipps, K. W. *J. Phys. Chem.* **1995**, *99*, 6684.
- (45) Manness, K. M.; Terrill, R. H.; Meyer, T. J.; Murray, R. W.; Wightman, R. M. *J. Am. Chem. Soc.* **1996**, *118*, 10609.

- (46) Anariba, F.; McCreery, R. L. *J. Phys. Chem. B* **2002**, *106*, 10355.
- (47) Solak, A. O.; Ranganathan, S.; Itoh, T.; McCreery, R. L. *Electrochem. Solid-State Lett.* **2002**, *5*, E43.
- (48) Ranganathan, S.; McCreery, R. L.; Majji, S. M.; Madou, M. J. *Electrochem. Soc.* **2000**, *147*, 277.
- (49) Ranganathan, S.; McCreery, R. L. *Anal. Chem.* **2001**, *73*, 893.
- (50) Anariba, F.; DuVall, S.; McCreery, R. L. *Anal. Chem.* **2003**, *75*, in press.
- (51) Kariuki, J. K.; McDermott, M. T. *Langmuir* **2001**, *17*, 5947.
- (52) Liu, Y.-C.; McCreery, R. L. *Anal. Chem.* **1997**, *69*, 2091.
- (53) Itoh, T.; McCreery, R. L. *J. Am. Chem. Soc.* **2002**, *124*, 10894.

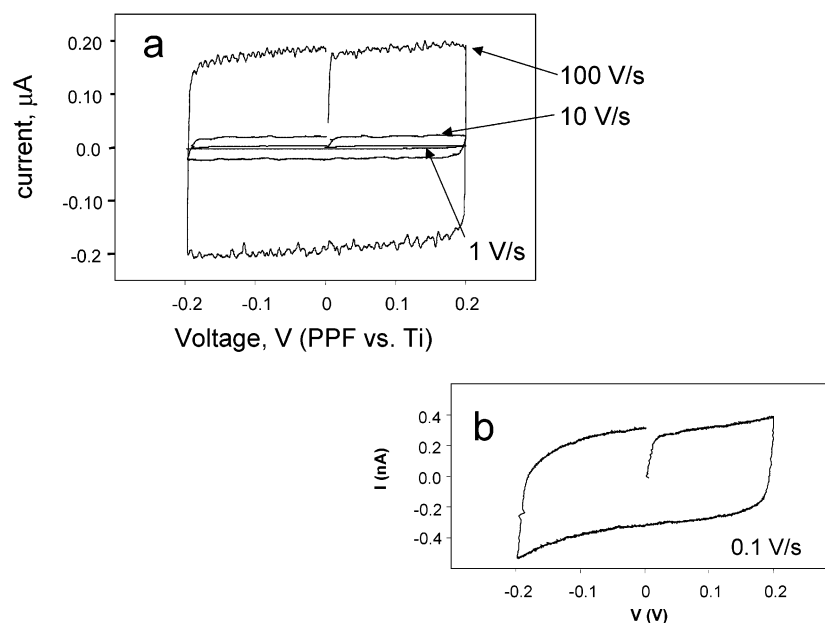


Figure 1. Voltammograms for a PPF/NAB(3.7)/Ti junction (area = 0.00785 cm²) for a ± 0.2 V range. Plot a shows i/V curves obtained at 1, 10, and 100 V/s; curve b is at 0.1 V/s. Positive current corresponds to electrons flowing from the Ti to the PPF, through the NAB layer. All voltages are stated as the PPF potential relative to the Ti contact.

By analogy to similar multilayers formed from diethylaminophenyl diazonium reagents,^{51,54} the NAB molecules are presumably linked to each other by bonds between phenyl rings. After derivatization, the entire Si/PPF/monolayer sample was rinsed with acetonitrile that had been purified with activated carbon and filtered through 0.2 μ m Millipore filters.

Immediately after rinsing, the PPF sample with NAB monolayer was placed behind a contact mask consisting of 0.5 or 1.0 mm diameter holes in a 1/32 in. thick polystyrene sheet. The mask and sample were positioned on a rotating holder in the top of an electron beam evaporator chamber, facing down, approximately 50 cm from a crucible containing metallic titanium. Titanium has been used previously as a metallic contact for both semiconductor and molecular junctions in part because of its high reactivity.^{29,55} An automated electron beam apparatus (Telemark, Fremont, CA) vaporized Ti from the crucible with the beam current operating near the threshold for Ti evaporation. The current was controlled to yield a Ti deposition rate at the sample of 0.03 nm/s until a thickness of 3 nm resulted, and then the deposition was paused for 5 min to permit cooling. An additional 10 nm of Ti was then deposited at 0.1 nm/s, and then an additional 40 nm at 1.0 nm/s. Metal thickness was monitored in situ with a quartz crystal microbalance positioned next to the sample (Telemark Model 860 deposition controller). The approximate velocity of the evaporated Ti atoms was measured separately by passing the Ti beam through a rotating 1 mm diameter aperture and noting the displacement of the Ti spot on a target as a function of rotation speed. The result was an average velocity of 71 ± 13 m/s. Although this velocity corresponds to a kinetic energy of <0.01 eV per Ti atom, the heat of condensation of Ti (~ 4 eV/atom) is much larger, and slow Ti deposition is essential to minimize sample heating. Following Ti deposition and without breaking the vacuum, Au was deposited through the same mask at 1.0 nm/s for a Au thickness of 100 nm. The gold layer prevented oxide formation on the titanium and permitted good electrical contact. The vacuum was cryopumped to $<8 \times 10^{-6}$ Torr during deposition, and the chamber temperature increased gradually from 15 to 25 $^{\circ}$ C due to heating by the e-beam crucible. The seven circular junctions were contacted individually using 220 μ m diameter platinum wire positioned with a

three-axis micropositioner and a macro video camera. The quality of the wire/Au contact was evaluated by placing the wire on 19 positions chosen randomly on a given Au spot, without any special control of wire pressure. The relative standard deviation of the junction resistance for these 19 contacts was 13%, implying that the force and position of the contact are not critical factors affecting the magnitude of the junction resistance. Contact to the PPF was made by piercing the NAB layer with a ~ 0.5 mm diameter metal spike at a position several millimeters laterally away from the Au/Ti junction.

NAB deposition and slow scan voltammetry were carried out with commercial potentiostats (Epsilon and BAS100 from Bioanalytical Systems, West Lafayette, IN), and fast electrochemical experiments were conducted with Labview software and data acquisition board (National Instruments, see Supporting Information for details). All voltammetric and pulse experiments were conducted at room temperature (22–24 $^{\circ}$ C), except for those reported in Figure 8, for which the sample was cooled in a plexiglass box under a stream of liquid nitrogen boiloff and the temperature was monitored with a thermocouple.

Raman spectroscopy was carried out in air at 514.5 nm, with a custom CCD spectrometer described previously,⁵⁶ and in the Supporting Information. XPS was conducted with a Kratos Axis Ultra spectrometer, as described in the Supporting Information. A Linux based dual Pentium PC workstation conducted various molecular modeling calculations using Gaussian 98,⁵⁷ with the B3LYP method and 6-31G(d) basis set.

Results

Junctions will be identified as PPF/NAB(3.7)/Ti to clearly denote the NAB layer thickness of 3.7 nm. Figure 1a shows a

(54) Kariuki, J. K.; McDermott, M. T. *Langmuir* **1999**, *15*, 6534.

(55) Konstadinidis, K.; Zhang, P.; Opila, R. L.; Allara, D. L. *Surf. Sci.* **1995**, *338*, 300.

(56) Ramsey, J. D.; Ranganathan, S.; Zhao, J.; McCreery, R. L. *Appl. Spectrosc.* **2001**, *55*, 767.

(57) Frisch, M. J.; Trucks, G. W.; Schlegel, H. B.; Scuseria, G. E.; Robb, M. A.; Cheeseman, J. R.; Zakrzewski, V. G.; Montgomery, J. J. A.; Stratmann, R. E.; Burant, J. C.; Dapprich, S.; Millam, J. M.; Daniels, A. D.; Kudin, K. N.; Strain, M. C.; Farkas, O.; Tomasi, J.; Barone, V.; Cossi, M.; Cammi, R.; Mennucci, B.; Pomelli, C.; Adamo, C.; Clifford, S.; Ochterski, J.; Petersson, G. A.; Ayala, P. Y.; Cui, Q.; Morokuma, K.; Malick, D. K.; Rabuck, A. D.; Raghavachari, K.; Foresman, J. B.; Cioslowski, J.; Ortiz, J. V.; Baboul, A. G.; Stefanov, B. B.; Liu, G.; Liashenko, A.; Piskorz, P.; Komaromi, I.; Gomperts, R.; Martin, R. L.; Fox, D. J.; Keith, T.; Al-Laham, M. A.; Peng, C. Y.; Nanayakkara, A.; Gonzalez, C.; Challacombe, M.; Gill, P. M. W.; Johnson, B.; Chen, W.; Wong, M. W.; Andres, J. L.; Gonzalez, C.; Head-Gordon, M.; Replogle, E. S.; Pople, J. A. *Gaussian 98*, revision A.7; Gaussian, Inc.: Pittsburgh, PA, 1998.

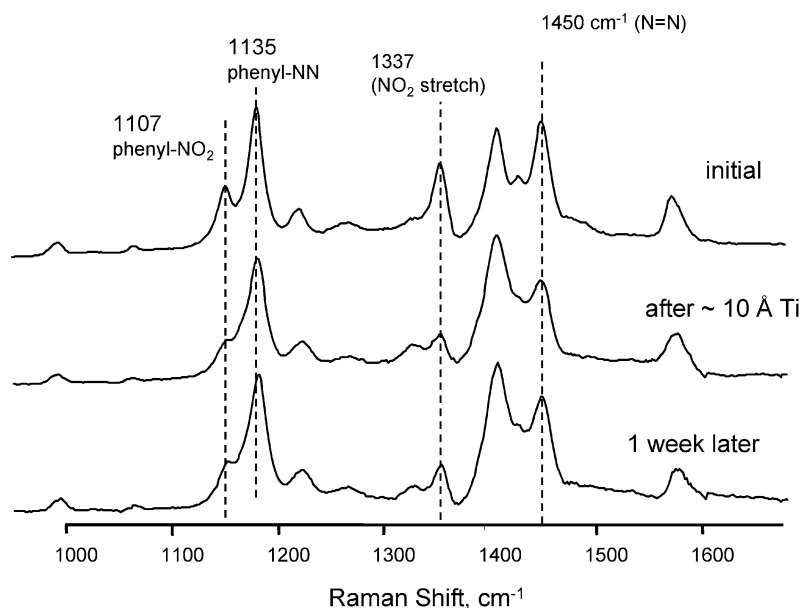


Figure 2. Raman spectra of a 3.7 nm film of NAB on PPF before and after deposition of 1 nm (average thickness) of Ti by e-beam evaporation at 0.03 nm/s. Laser power at sample was 45 mW over a 0.05×5 mm line focus;⁵⁶ integration time was 30 s in all cases. The “initial” spectrum was obtained from a region not exposed to Ti; middle spectrum was obtained within 1 h after Ti deposition; lower spectrum was obtained after 1 week in air. A spectrum of unmodified PPF was subtracted in all cases.

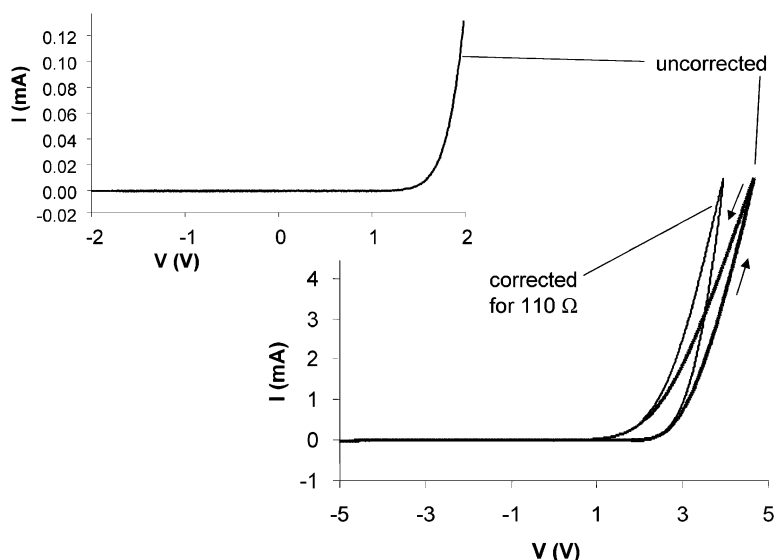


Figure 3. Wide scan (-5 to $+4.6$ V) i/V curves for a PPF/NAB(37)/Ti junction (area = 0.00196 cm²), scan rate of 1 V/s. Upper panel shows ± 2 V range with expanded current scale. Arrows show scan direction, and “corrected” curve has a voltage scale corrected for 110Ω of series resistance in the PPF substrate. Voltage axis is PPF relative to Ti.

representative set of i/V curves obtained at 1–100 V/s, which exhibit both a capacitive and a resistive component. The low voltage resistance (± 50 mV) was measured as the inverse of the slope of the i/V curve obtained at 0.1 V/s (Figure 1b), which is ~ 1 G Ω in this case. To permit comparison of junctions with different areas, the junction resistance is often stated as the product of resistance and area, yielding ~ 8 M Ω cm² in the case shown. For approximately 24 h after metal deposition, the junction resistance increased from <100 K Ω to >10 M Ω for a 0.5 mm diameter junction. For example, the mean and standard deviation of seven junctions on the same sample increased from 38 ± 18 k Ω to 249 ± 46 M Ω over a 6 day period (daily observations for all seven junctions are listed in Supporting Information, Table S1). Results for 67 junctions on 12 samples prepared by three different researchers are listed in Table 1 for

junctions that were at least 1 week old. After several days of increasing resistance, the junction resistance became stable for at least 2 months.

Raman spectroscopy was used to probe possible structural changes accompanying the changes in junction resistance following metal deposition. NAB has relatively strong Raman scattering on carbon surfaces when observed with a high-sensitivity spectrometer,⁵⁶ and the spectrum has been analyzed in detail.⁵³ To probe the NAB layer spectroscopically, the metal deposition was stopped after an initial ~ 1 nm thick Ti layer. This Ti layer is partially transparent and attenuates the NAB surface Raman intensity by less than 10%.

Although the unprotected Ti layer partially oxidizes upon exposure to air, its transparency permits spectral analysis of the underlying NAB layer. Figure 2 shows Raman spectra of a 3.7

Table 1. Junction Resistance and Capacitance

sample	junctions	<i>R</i>		<i>C</i>		<i>i</i> (+3 V)	
		MΩ cm ²	% rsd	μF/cm ²	% rsd	A/cm ²	% rsd
022103 A	6/6 ^a	4.81 ^b	29	0.907 ^c	4	0.443	40
022103 A	6/6	3.66	67	0.943	5	0.502	29
022103 C	5/7	2.07	88	0.947	20	0.517	48
022803A	11/11	2.88	87	0.985	5	0.447	71
022803B	4/7	1.19	84	1.074	17	0.841	50
022803C	5/7	4.58	33	1.191	4	1.113	18
040503A	6/8	1.94	19	1.257	9	0.910	14
040503C	5/9	1.94	56	1.176	11	1.077	24
041503-7	7/7	3.74	21	1.29	7	1.59	19
041503-8	6/7	4.68	57	0.83	17	0.55	31
040303-CY2	3/4	3.63	66	1.344	8	1.020	22
040303-CY4	3/3	3.12	48	1.150	1	0.886	18
mean of 12 samples	67/82 ^e	4.07		1.088		0.754	

^a Number of junctions averaged/total number on sample. Junctions with anomalously low resistance were rejected. ^b Product of observed resistance and junction area. Resistance determined as the inverse slope of the *i*/*V* curve from −50 to +50 mV at a scan rate of 0.1 V/s. ^c All capacitance values listed were determined at 1 V/s. ^d Scan rate = 1 V/s. ^e Total of 67 junctions were averaged, out of 82 junctions on 12 samples. Rejection was based on a low voltage resistance less than 1 MΩ for a 1 week old junction.

nm thick NAB layer on PPF before (top spectrum) and after (middle spectrum) deposition of 1.0 nm of Ti. A spectrum of the PPF substrate was subtracted in all cases, to remove the broad PPF bands at ~1360 and ~1600 cm^{−1}. The analysis of these spectra will appear in detail elsewhere, but the main Raman features are identified in Figure 2. Upon Ti deposition, three Raman bands associated with normal modes which involve the nitro group decrease significantly in intensity for the spectrum obtained ~1 h after Ti deposition. These features partially recover their intensity over a period of several days, returning to about 40% of their initial intensities relative to the other bands. As discussed below, we attribute this recovery to reoxidation (presumably by air) of NAB reduced during deposition of titanium. The remainder of the spectrum is not drastically affected by Ti deposition, implying that the NAB layer is largely intact. The recovery of the 1337 and 1450 cm^{−1} bands during “aging” approximately tracks the observed increase in junction resistance. XPS of the 1.0 nm Ti/NAB/PPF sample reveals a Ti–N feature at 397.0 eV and a decrease of the 406 eV N_{1s} feature corresponding to the NO₂ group.

Figure 1 includes *i*/*V* curves for a PPF/NAB(3.7)/Ti junction obtained at scan rates of 1, 10, and 100 V/s. The current at 0 V was used to determine the observed junction capacitance by dividing by the scan rate, yielding 0.82 μF/cm² at 100 V/s in the case shown. The capacitance was quite reproducible for different junctions both on the same sample and between samples, with standard deviations in the range of 4–20%. Table 1 includes junction capacitance values for 67 PPF/NAB(3.7)/Ti junctions, showing a range of 0.91–1.26 μF/cm² for a scan rate of 1 V/s. The capacitance typically decreased with increasing scan rate, indicating the presence of frequency dispersion which is not expected for an ideal parallel plate capacitor. For example, the capacitance of a typical junction decreased from 1.17 μF/cm² at 0.1 V/s to 0.52 μF/cm² at 100 V/s.

Figure 3 shows a wide scan *i*/*V* curve for a PPF/NAB(3.7)/Ti junction acquired at 100 V/s, scanning from 0 to −5 V, and then to +4.6 V. The heavy curve is the raw data and shows both rectification and hysteresis. The current at 4.6 V is 538 times as large as that at −4.6 V, and the peak current density

was 3.2 A/cm² at +4.63 V. The average electric field across the NAB layer at the scan limits is very large, about 12 MV/cm in this case. The differential resistance (*dE*/*di*) at the peak on the forward scan is 221 Ω, as compared to ~600 MΩ observed near 0 V. The large currents near the peak result in significant ohmic potential error from the PPF and contact resistance. The lighter curve in Figure 3 was obtained after correcting the applied voltage by the *iR* drop through a 110 Ω background resistance in series. 110 Ω is the mean of control experiments in which the NAB layer was absent, but the standard deviation of control values was high, generally greater than 50%. The correction indicates that the *i*/*V* curve may be steeper than it appears in the raw data, implying a quite low contribution by NAB to the junction resistance. An *i*/*V* scan between −3 and +3 V showed similar rectification and could be repeated hundreds of times without observable degradation. The inset of Figure 3 shows an uncorrected ±2 V scan, for which the current is smaller and less subject to ohmic potential error. The observed ratio of the current magnitude at +2 V to that at −2 V was 608 for this case.

Figure 4 shows the dependence of the *i*/*V* curve on scan rate ranging from 1 to 1000 V/s and starting at both −3 and +3 V. The upper panel shows *i*/*V* curves initiated after holding at −3 V for 3 s. For the 1000 V/s scan rate, the hysteresis is quite small, as is the current at +3 V. As the scan rate decreases to 1 V/s, more hysteresis is observed, and the current at +3 V increases. When the scan rate is initiated in a negative direction after holding the potential at +3 V for 3 s, the response is independent of scan rate at positive potentials, but shows a transient negative current at negative potentials for the higher scan rates.

Inspection of Figure 4 reveals that hysteresis is observed for both positive and negative potentials, but the direction of the hysteresis differs. The magnitude of the current increases while scanning through potentials more positive than 2 V, while it decreases for potentials more negative than −2 V.

To investigate the hysteresis in more detail, the current response to potential pulses was determined for various pulse durations and magnitudes. Figure 5 shows current transients for voltage pulses between 0 and +3 V and 0 and −3 V on quite different current scales. The +3 V pulse generates a rapid transient current lasting a few milliseconds, followed by a relatively slow increase to a few milliamperes lasting at least 1 s. After 100 ms at +3 V, the current is about 500 times that after 100 ms at −3 V, consistent with the rectification shown in Figure 3. The origin of the rapid transient decrease, shown in detail for a 1 ms, +3 V pulse shown in panel 5c, is the subject of ongoing study. The current amplifier response distorts the results for periods of <10 μs after a potential change, but a clear current transient is observed for both the rising and the falling sides of a square voltage pulse. A plot of ln(*i*) versus *t* for either the positive or the negative slope of a 1 ms, +3 V pulse (panel 5d) did not exhibit the linearity expected for RC charging. The slow current increase corresponds to the hysteresis observed in Figures 3 and 4, because a potential step to +3 V yields an immediate current equal to *i*(+3 V) on the lower *i*/*V* curve at a given scan rate followed by a slow rise to *i*(+3 V) on the upper *i*/*V* curve. The slower scan rates used for the *i*/*V* curve yield larger currents in the positive region (Figure 4) because more time is permitted for the “slow” current in-

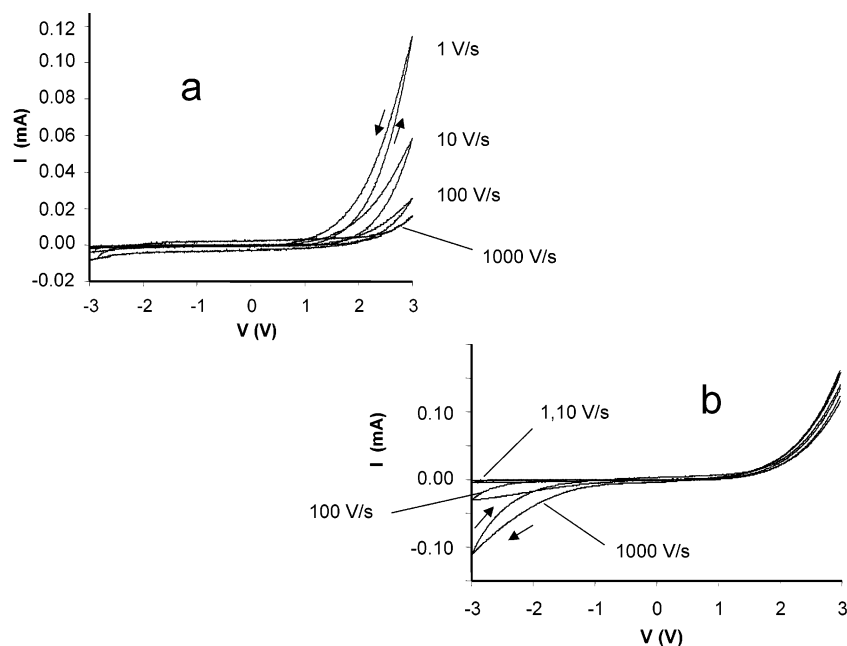


Figure 4. ± 3 V i/V curves for several scan rates, initiated at -3 V (a) or $+3$ V (b). Arrows indicate scan direction, and scan rates are indicated. Junction area = 0.00196 cm^2 . Voltage axis is PPF relative to Ti.

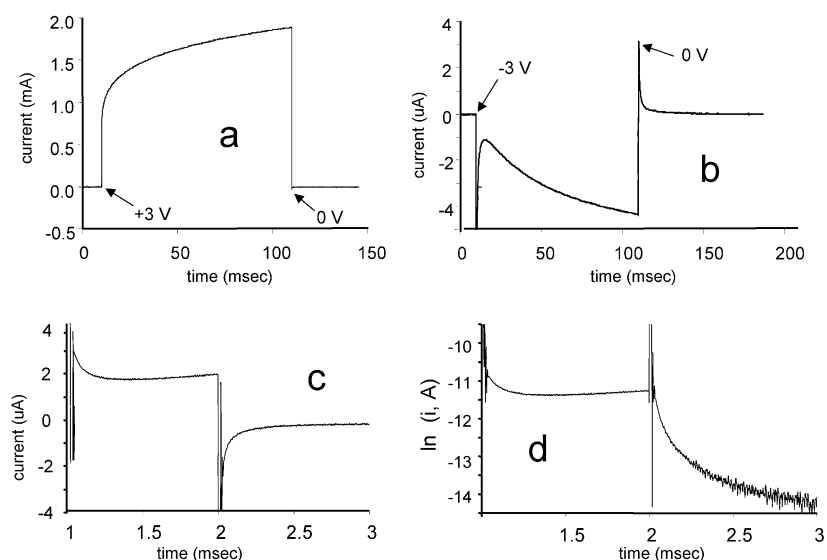


Figure 5. Current transients resulting from square voltage pulses to $+3$ or -3 V, starting at $V = 0$ (junction area = 0.00785 cm^2). Panel a: 100 ms pulse from 0 to $+3$, then back to $V = 0$. Panel b: 0 to -3 V pulse at much higher sensitivity. Panel c: 1 ms pulse from 0 to $+3$ V ($t = 1\text{--}2$ ms, then back to $V = 0$). Panel d: plot of $\ln|i|$ vs t for data in panel c. Note the large differences in current and time scales.

crease. The hysteresis and transient response clearly indicate a dynamic junction on at least two time scales: <10 ms and $10\text{--}1000$ ms.

The potential dependence of the transient response is shown in Figure 6a for 100 ms pulses from 0 V to varying positive voltages. For the “forward” pulse (100–200 ms) in Figure 6, the current magnitude and rate of increase are strongly dependent on potential. The “slow” current increase is larger and faster as the potential increases above 2 V. The “reverse” transient obtained when the potential returns to 0 V (200–250 ms) is quite informative, and a magnified view is shown in Figure 6b. Because the applied voltage is zero, the junction is short-circuited, and the current represents charge ejected into a short circuit. In effect, the junction is acting as a small battery, and the area under the backstep transient is the charge stored in the

battery. The RC time constant for a series resistance of 110Ω and a capacitance of $1 \mu\text{F}/\text{cm}^2$ is less than $1 \mu\text{s}$, so the transients do not result solely from the discharge of a parallel plate capacitor. Figure 6 also includes a plot of the area under the backstep ($V = 0$) current transient converted to moles/ cm^2 by dividing by Faraday’s constant and the junction area. For 100 ms pulses, the observed backstep charge is small until the forward voltage exceeds 1 V, and then it increases to approximately 6×10^{-10} moles/ cm^2 after a $+4$ V pulse.

The NAB (3.7) junctions did not immediately return to their initial states after a positive potential pulse, as shown in Figure 7. After an initial i/V scan at 1000 V/s, a 1 s, $+4$ V pulse was applied. The junction then remained at 0 V except for additional 1000 V scans at 1 s, 1, 3, 6, and 60 min after the end of the pulse. The voltammetric current immediately following the

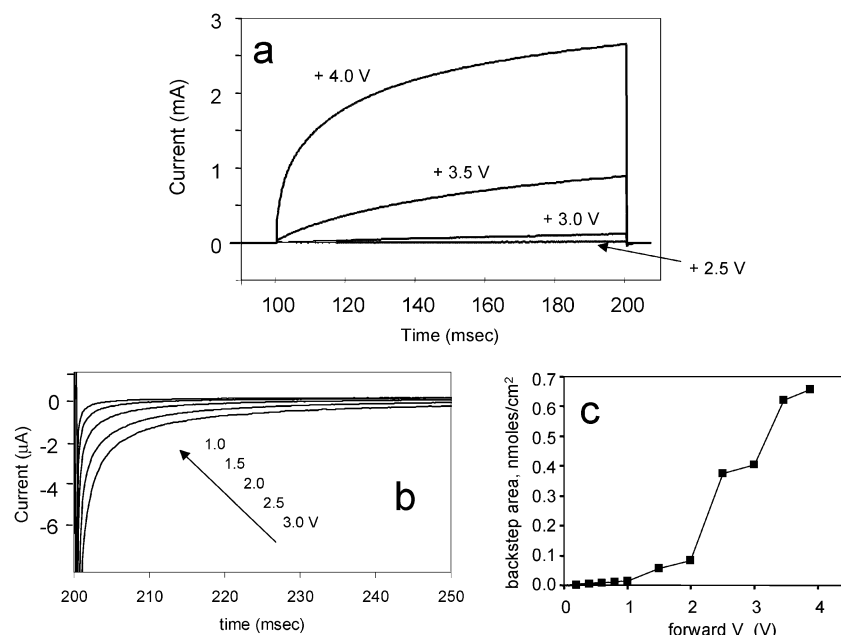


Figure 6. Response to 100 ms voltage pulses from $V = 0$ to various positive potentials (junction area = 0.00785 cm²). Panel a: Four transients for pulse heights of 2.5, 3.0, 3.5, and 4.0 V. A slow “reset” scan from 0 to -2 V (0.25 V/s) preceded each pulse. Panel b: Current response to a potential step from a positive voltage (as indicated) to $V = 0$. Lower curve is the backstep from +3 V; upper curve is from +1 V. Note the change in sensitivity as compared to panel a. Panel c: integrated areas of current transients similar to those in panel b, expressed as nanomoles of electrons/cm².

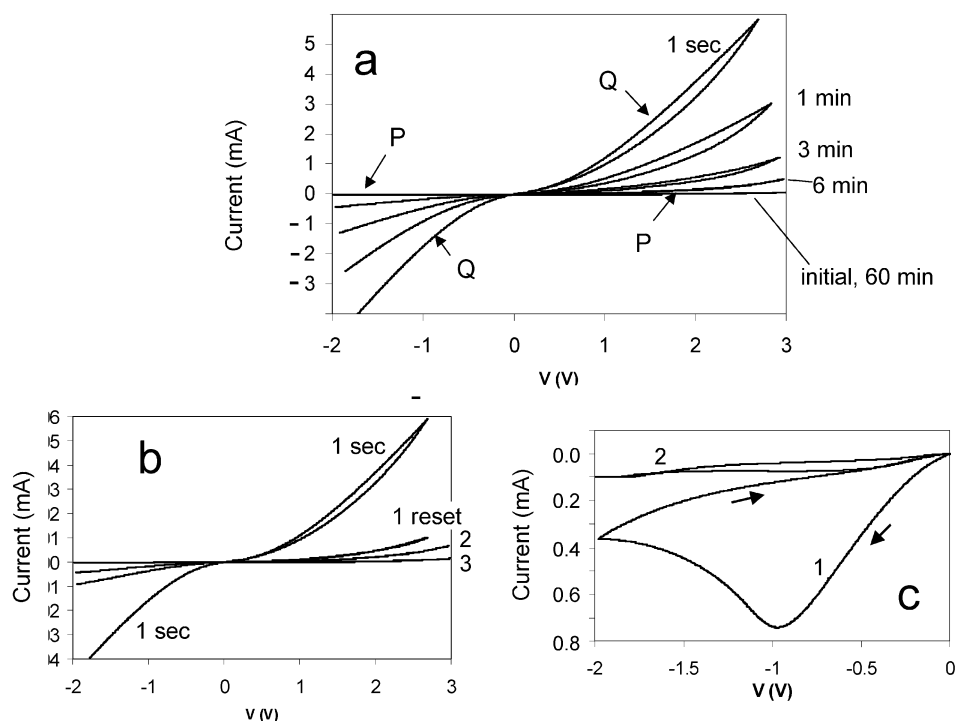


Figure 7. Evolution of i/V curves after a +4 V, 1 s pulse and return to $V = 0$. Panel a: i/V curves obtained at 1000 V/s at times of 1 s, 1, 3, 6, and 60 min after +4 V pulse, with junction held at $V = 0$. The i/V curves before the pulse and 20–60 min after the pulse were superimposable. The curve marked “Q” is characteristic of the “quinoid”, or reduced, form of NAB, and that marked “P” is characteristic of the “phenyl”, or oxidized, form. Panel b: 1000 V/s curves obtained 1 s after +4 V, 1 s pulse, and after one, two, and three “reset” scans (0 to -2 V, 0.25 V/s). Each reset scan required <20 s, and the first two are shown in panel c.

pulse (curve Q in Figure 7a) was large (>0.6 A/cm² at +3 V), but decreased with time until it returned to the initial value after about 10 min (curve P). The decrease in current was accelerated significantly by a “reset” scan consisting of a 0 V to -2 V to 0 V sweep at 0.25 V/s. After one reset scan requiring <20 s, the current at +3 V decreased by 83%, while

a 20 s wait at $V = 0$ decreased the current by only about 20% (Figure 7a). The low voltage resistance increased after each reset scan, with a value of about 2 K Ω immediately after the +4 V pulse, increasing to 65 K Ω after five reset scans. Two reset scans are shown in Figure 7c, as well as the resulting i/V curves in Figure 7b.

Finally, the effect of temperature was examined for ± 5 V scans obtained at 100 V/s. Figure 8a shows i/V curves obtained at 24, -17 , and -137 °C, with Figure 8b showing the 0 to $+5$ V range with an expanded current scale. At the lower temperature, the current increase for positive potentials was much smaller, and the hysteresis was absent below about -100 °C. The 24 °C curve was restored after the junction was allowed to warm to room temperature.

Discussion

Junction capacitance provides an initial measure of the reproducibility of PPF/NAB(37)/Ti junction fabrication, as well as a test of junction structure.^{13,58} The 4–20% relative standard deviations (rsd) of capacitance (1 V/s) for 12 samples (Table 1) indicate reasonable uniformity of junction thickness. Using a simple parallel plate model for the junction capacitance, the observed value of $1.09 \mu\text{F}/\text{cm}^2$ and measured layer thickness of 3.7 nm yield a dielectric constant of the molecular layer of 4.4. Dielectric constants for thin, oriented molecular films are generally unknown, but a relevant range includes those for bulk polystyrene (2.0), liquid nitrobenzene (35), and alkane thiol SAMs (2.5).^{13,58} Although a dielectric constant of 4.4 is reasonable, it should be interpreted with caution due to the observed dependence of capacitance on frequency. The rsd of junction resistance was higher, possibly due to defects or to “stray” electrons remaining in the NAB film (see below). The relatively high yield of functional junctions was somewhat unexpected, given difficulties reported for fabrication of Au/thiol/metal, Langmuir–Blodgett, and PPF/molecule/Hg junctions.^{15,25,27,46,59} The PPF–NAB bond is strong (~ 100 kcal/mol) and is formed irreversibly, and hence it should be less prone to damage during Ti deposition. Furthermore, we chose a relatively thick molecular layer (3.7 nm) to reduce the chance of pinhole defects and short circuits. As shown by Kariuki and McDermott,^{51,54} multilayers may form during diazonium deposition by attack of the first monolayer by electrogenerated phenyl radicals to form a phenyl–phenyl bond. Although a 3.7 nm NAB layer is presumably less ordered than a monolayer (~ 1.5 nm), it can be considered a short oligomer of 2–3 NAB subunits.

The Raman and XPS results clearly indicate a strong interaction between Ti and the NO_2 group of NAB. Ti atoms are strong reducing agents due in part to their high free energy in the vapor phase. The change in the Raman spectrum upon Ti deposition (Figure 2) causes a decrease in all of the bands associated with the nitro group.^{53,60} However, these bands partially recover on a 1–5 day time scale, implying that the NAB is reduced by deposited Ti, and then partially reoxidized, presumably by air. The observation of a Ti–N XPS feature indicates a covalent bond between the NAB and titanium, which persists indefinitely. Chemisorption of nitrobenzene to Ni and Fe surfaces in UHV has been shown to yield a metal–nitroso linkage,^{61,62} and such a bond is a possibility for the Ti/NAB interface studied here. The partial recovery of the nitro group Raman features implies that the top of the NAB layer reacts

irreversibly with the Ti, while interior nitro groups can be reoxidized. Detailed Raman and XPS spectroscopy of PPF/NAB/metal junctions will be reported separately, but the current results are consistent with a 3.7 nm NAB layer covalently bonded to both the PPF via a C–C bond and the Ti by a Ti–N bond. Allara et al. have reported that reactive end groups on Au/SAM monolayers help prevent incursion of vapor deposited silver into the SAM,^{59,63,64} and a similar end-group reaction is indicated for the PPF/NAB/Ti junctions in the current investigation. Although residual water, acetonitrile, or electrolyte should have been removed by rinsing and exposure to vacuum, it is possible that ions were generated upon Ti deposition, or during application of an external voltage. The combination of a stable, densely packed molecular layer with strong covalent bonds to the substrate, low energy Ti atoms resulting from near-threshold operation of the e-beam evaporator, and a reaction between Ti atoms and nitro groups appears responsible for the high yield of molecular junctions despite their relatively large 0.5–1 mm diameter. Presumably due to the very high aspect ratio of the molecular layer ($\sim 10^6$) and a Au–Ti top contact much thicker than the molecular layer, junctions did not appear to be damaged by repeated mechanical contact by the external lead to the Au pad.

The correlation of the increase in junction resistance for ~ 24 h after Ti deposition with the partial recovery of the NO_2 peaks in the Raman spectra provides an important clue to the junction’s electronic behavior. We reported previously that electron injection into conjugated monolayers results in a significant conductivity increase that was manifested in electrochemical experiments.⁶⁵ Furthermore, reduction of NAB monolayers on carbon surfaces monitored in situ with Raman spectroscopy in an electrochemical cell permitted detailed structural analysis of the reduced NAB resulting from electron injection.⁵³ Injection of electrons by condensing Ti atoms into NAB should result in partial or complete reduction of the NAB, and a similar increase in conductivity may occur. The low initial junction resistance may reflect the “reduced” NAB state, as do the weak intensities of Raman bands associated with the NO_2 group. The proposal of a conductivity change caused by e^- injection is substantiated below, but the Raman spectra provide a correlation of NAB reduction and increased conductivity.

The i/V curves in Figures 3, 4, and 8 permit several conclusions about electron transport through the 3.7 nm NAB film after the initial “aging” period of about 1 week. The mechanism underlying the large currents for $V > 2$ V is both time and temperature dependent, implying a chemical transformation involving nuclear rearrangement and an activation barrier. The strong scan rate dependence (Figure 4) and transient response (Figures 5, 6) indicate a process with a 10–1000 ms time scale. If this process is prevented by a fast scan rate or low temperature, the increase in current is much smaller or not observed at all. For the junction shown in Figure 8, the current density at $+3$ V decreases from $0.58 \text{ A}/\text{cm}^2$ at 24 °C to $0.0012 \text{ A}/\text{cm}^2$ at -137 °C. The mean current density observed at room temperature, $0.71 \text{ A}/\text{cm}^2$, corresponds to $10^5 e^-/\text{s}/\text{molecule}$,

(58) Haag, R.; Rampi, M. A.; Holmlin, R. E.; Whitesides, G. M. *J. Am. Chem. Soc.* **1999**, *121*, 7895.

(59) Fisher, G. L.; Hooper, A. E.; Opila, R. L.; Jung, D. R.; Allara, D. L.; Winograd, N. *J. Phys. Chem. B* **2000**, *104*, 3267.

(60) Biswas, N.; Umapathy, S. *J. Phys. Chem. A* **2000**, *104*, 2734.

(61) Kishi, K.; Chinomi, K.; Inoue, Y.; Ikeda, S. *J. Catal.* **1979**, *60*, 228.

(62) Campion, A.; Brown, J. K.; Grizzle, V. M. *Surf. Sci. Lett.* **1982**, *115*.

(63) Fisher, G. L.; Hooper, A.; Opila, R. L.; Jung, D. R.; Allara, D. L.; Winograd, N. *J. Electron Spectrosc. Relat. Phenom.* **1999**, *98–99*, 139.

(64) Hooper, A.; Fisher, G. L.; Konstadinidis, K.; Jung, D.; Nguyen, H.; Opila, R.; Collins, R. W.; Winograd, N.; Allara, D. L. *J. Am. Chem. Soc.* **1999**, *121*, 8052.

(65) Solak, A. O.; Eichorst, L. R.; Clark, W. J.; McCreery, R. L. *Anal. Chem.* **2003**, *75*, 296.

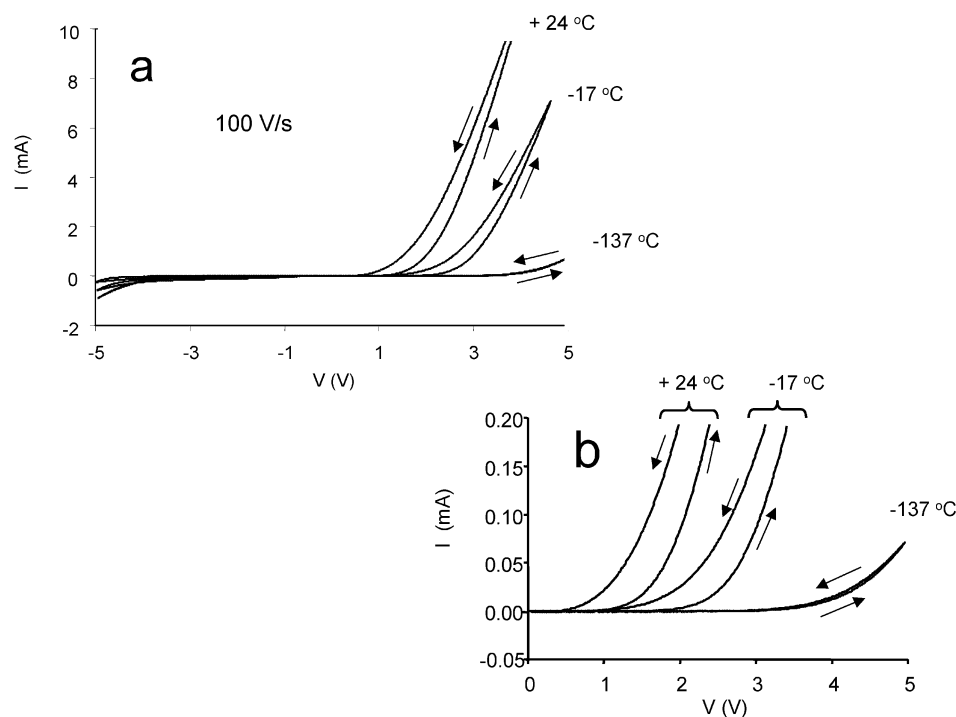


Figure 8. Effect of temperature on i/V curves (100 V/s, 0 to +5 to -5). Arrows indicate scan direction, with scans initiated at $V = 0$ in the positive direction. Junction area was 0.00785 cm^2 .

assuming a coverage of $4 \times 10^{-10} \text{ moles/cm}^2$. In addition to being time and temperature dependent, the currents observed for a positive voltage are strongly potential dependent, as shown in Figures 5 and 6. Negative pulses to -3 V produce small current transients, but positive pulses produce current transients which increase in magnitude with potential above $+2 \text{ V}$. Both the plateau current and the rate of increase are larger for more positive potentials. Once the large current increase for positive potentials is achieved, the high conductivity state relaxes slowly, requiring several minutes at $V = 0$ (Figure 7a) to return to the state which preceded the pulse. The i/V curve marked “Q” in Figure 7a was obtained for the junction resulting from a 1 s , $+4 \text{ V}$ pulse; curve “P” is the i/V curve before the $+4 \text{ V}$ pulse, or after 60 min of waiting at $V = 0$ or accelerating relaxation with negative scans (Figure 7b).

The small negative current spikes apparent in Figure 6a and magnified in 6b are critical to understanding the nature of the conductivity change. Because these spikes occur with zero applied voltage, they do not result from junction conductivity, per se. Instead, the junction is acting as a small battery that is discharging into an effective short circuit. The area of these transients represents charge expelled from the junction after the applied voltage is removed. If the spikes were caused solely by discharge of the junction capacitance, they should be much shorter ($RC \approx 0.4 \mu\text{s}$) and too fast for the data acquisition system to monitor. The observed backstep transient lasts $>40 \text{ ms}$ following a 100 ms positive pulse, and the integrated area is $(4\text{--}7) \times 10^{-10} \text{ moles/cm}^2$ for $3\text{--}4 \text{ V}$ positive pulses (Figure 6c). The results shown in Figure 6b and 6c clearly indicate that charge is injected into the junction when a positive potential is applied, and then ejected when $V = 0$. Taken together, the observations indicate that the current increase for positive potentials involves electron transfer into the NAB layer in response to the applied voltage. Electron injection is time

dependent, potential dependent, and thermally activated, implying accompanying reorganization of nuclei in the NAB layer. The amount of charge is approximately equivalent to a monolayer ($\sim 4 \times 10^{-10} \text{ moles/cm}^2$) or about $10^{20} \text{ e}^-/\text{cm}^3$ for a 3.7 nm NAB film.

Although there is no direct evidence for the presence of ions other than NAB^- in the PPF/NAB/Ti junctions, ions may be involved in the slow response to voltages above $+2 \text{ V}$. By analogy to redox polymer films, electron injection into the NAB may be accompanied by motion of adventitious ions generated during junction fabrication or by the applied voltage. For example, it is conceivable that the applied voltage causes chemical reactions at the Ti/NAB interface which generate mobile ions. Such ions may redistribute in the electric field, requiring time for mass transport and possibly contributing to the slow time response. Such ion motion, if present at all, cannot be the sole source of the large junction conductivity, which is orders of magnitude higher than any conceivable ionic current. However, the current results do not rule out the possibility of ion motion in the NAB film, and such motion may accompany the structural rearrangement which increases junction conductivity. Furthermore, it is also possible that holes rather than electrons are involved in the conductivity of the monolayer, although a precedent exists for electrochemical reduction of NAB,⁵³ and removal of an electron from NAB would be energetically less favorable.

At least conceptually, charge injection into the molecular layer accompanied by structural rearrangement bears similarities to an electrochemical redox process, but with the solvent and counterion absent. For example, an electrode modified with a redox active monolayer can inject electrons into the molecular layer, and the electron may “hop” between redox centers.³⁷ The resulting charge is neutralized by counterion motion toward the monolayer from solution, so the monolayer may be stable in

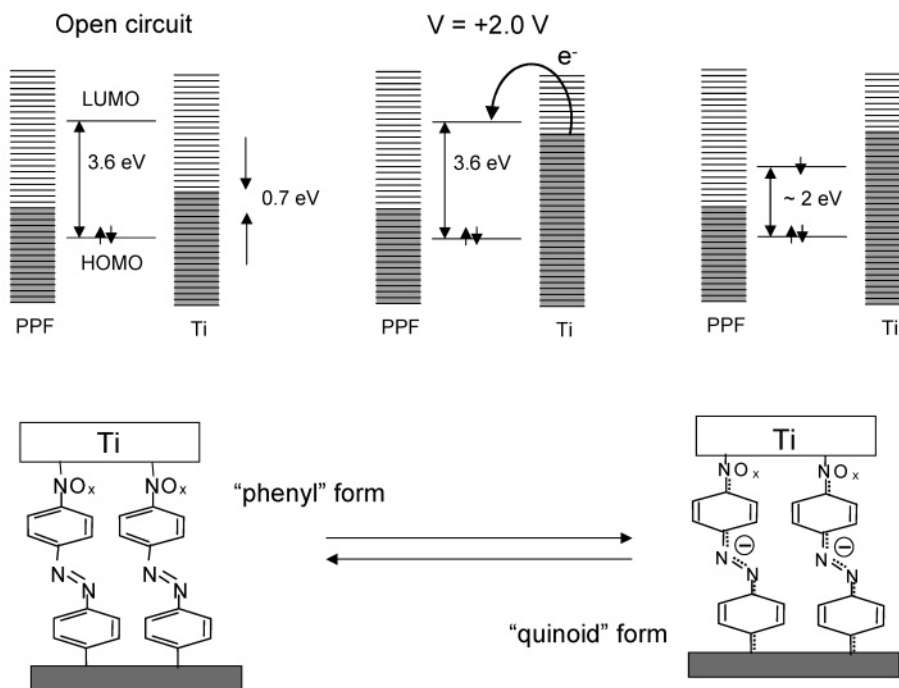


Figure 9. Proposed energy level diagrams and structures for the transition from the less-conducting “phenyl” form to the higher-conducting “quinoid” form of NAB. The quinoid structure is drawn to represent delocalized electrons and a net monoanionic charge. Shading in upper diagrams indicated filled electronic states in the PPF and Ti. See text for details.

either its oxidized or its reduced form. We reported recently that electron transfer to a solution redox species through nitrobiphenyl and biphenyl monolayers was much faster after electrons were injected into the modification layer.⁶⁵ In the current molecular junctions, charge injection is caused by the large imposed electric field, and the charged monolayer is stabilized by the nearby counter electrode. Once the electric field is relaxed, the stored charge leaves the junction and appears as the current transient in Figure 6b. For NAB, the activation barrier for the molecular rearrangement accompanying charge injection is apparently large enough to be responsible for the slow relaxation of the conductive state and to require significant potentials to drive electrons into the NAB. It is tempting to propose that the potential dependence of charge injection is an activated reaction governed by Marcus-like electron transfer kinetics, with the activation barrier height modified by the applied electric field. Because there is no reference potential, the process must be field driven, and the observed voltages do not correspond to a conventional redox potential scale. Marcus–Levich kinetics would indeed predict a faster rate for higher field, in addition to exponential temperature dependence. However, the nature of the barriers in the present junctions is not clear, and there may be several with different activation energies. A molecular rearrangement in the presence of a high static electric field may be governed by Marcus kinetics, but the relevant barrier may alternatively be at the molecule/Ti or molecule/PPF interfaces. The current results demonstrate that charge injection occurs, causes a conductivity change, and is temperature dependent, but they do not yet permit a particular kinetic model to be proposed.

A mechanism consistent with the observations is shown schematically in Figure 9 for the case of a NAB monolayer. Initially, assume minimal charge transfer between NAB and the contacts to yield the structure and energy diagram at the left in

Figure 9. The work function of Ti (4.3 eV) places its Fermi energy 0.7 eV higher than that of PPF (~5.0 eV). As is generally assumed, the HOMO–LUMO gap of the molecule straddles the Fermi levels of the contacts, and the calculated gap from Gaussian 98 for free NAB is 3.6 eV. When a positive potential is imposed on the PPF, the electrons in the Ti are destabilized and transfer into the NAB layer over an activation barrier involving NAB reorganization or an interfacial barrier, or both. The reduced NAB is an anion or methide, both of which have significant quinoid character.⁴⁷ Raman spectroscopy of NAB bonded to carbon surfaces in an electrochemical cell revealed decreases in the intensities of the nitro group vibrations similar to those observed following titanium deposition.⁵³ Furthermore, the spectroelectrochemical experiments provide support for the formation of a methide or anion via electron injection into NAB. The HOMO–LUMO gaps for the methide (2.1 eV) or anion (1.7 eV) are significantly smaller than that of NAB (3.6 eV) and are the likely cause of higher conductivity. The lower energy LUMO of the reduced NAB presents a lower barrier for electron tunneling or a lower energy conduction path for electrons. In addition, the high density of charge carriers in the NAB film (~10²⁰/cm³) stabilized by the reduced NAB and the applied field may be sufficient to maintain a significant steady state current. It is not yet clear whether a conductivity increase based on the presence of injected charge carriers or on the presence of a quinoid structure is the better model, but we expect the detailed study of temperature dependence currently underway to help clarify the conductivity mechanism in both the phenyl and the quinoid states.

Once electron injection occurs and the quinoid structure is formed, the NAB layer has low resistance and exhibits the *i/V* response labeled “Q” in Figure 7a. This conductive state persists as long as the electric field is imposed. If the applied voltage is returned to 0 V after a positive pulse generates the quinoid form,

the injected charge is ejected and the quinoid form reverts to the less conductive phenyl form. The return to the phenyl form may be accelerated by an imposed negative potential, which presumably drives electrons out of the layer and “reoxidizes” the quinoid form to the original NAB (Figure 7b). It is not clear at present why the current transient in Figure 6b occurs in less than 1 s, while the relaxation of the “Q” state requires several minutes at $V = 0$, but a possibility is that relatively few injected electrons are required for the observed conductivity increase. The area under the 0 V current transient represents the number of electrons responsible for the conductivity change. The observed value of $(6-7) \times 10^{-10}$ moles/cm² varies somewhat for different samples, but is approximately 0.1–1 e[−] per molecule of NAB in the film. The space charge resulting from these injected electrons is balanced by the large electric field and relaxes with accompanying molecular rearrangement when the field is removed. The proposal of charge injection leading to a conductivity change is similar to that reported for PPF/NAB/Hg junctions,^{14,65} but the polarity is reversed. The mercury junction became more conductive when the PPF was negative, and the “ON” state was more stable than that observed here. This difference may result from the higher work function of Hg (5.0 eV) as compared to Ti (4.3 eV), making e[−] injection from Ti energetically more favorable than that from Hg. In addition, the noncovalent contact at the NAB/Hg interface presumably generates a significantly higher barrier to electron transfer.

The mechanism proposed here, which is based on an activated molecular rearrangement, differs fundamentally from several theories proposed by others to explain molecular rectification and conductance switching.^{17,20,21,24,31,32} Most existing mechanisms rely on variations in the alignment of the Fermi levels of the contacts with molecular orbitals in the monolayer caused by changes in applied voltage.^{16,66,67} An example is resonant tunneling, in which the Fermi level of the contact emitting

electrons becomes aligned with the LUMO of the molecule, thus creating a low resistance conduction path.^{32,68} In addition, Hipps et al. have reported electron transfer through tunneling junctions at low temperature mediated by molecular orbitals in the junction.^{41,44,69} While mechanisms based on orbital alignment in an electric field are adequate to explain many molecular electronic effects, they would not be expected to be temperature dependent and are not sufficient to account for all of the PPF/NAB(3.7)/Ti junction properties. Ratner et al. have considered thermally induced hopping⁷⁰ and electron injection resembling thermionic emission⁷¹ for conduction through molecular junctions, both of which are temperature dependent. While such mechanisms may certainly be involved for the junctions studied here, they would not be expected to account for the observed kinetic behavior. The clear time and temperature dependence for the PPF/NAB(3.7)/Ti junctions require an activation step involving molecular reorganization which operates more favorably with positive bias. Detailed examination of the kinetics, temperature dependence, and thickness dependence of the PPF/NAB(3.7)/Ti junction conductivity and dynamics is currently in progress and is expected to significantly narrow the range of possible mechanisms of electron injection and transport.

Acknowledgment. This work was supported by the National Science Foundation through project 0211693 from the Analytical and Surface Chemistry Division, and by ZettaCore, Inc. The authors appreciated discussions with Mark Ratner and Werner Kuhr during the course of this work.

Supporting Information Available: Experimental details (PDF). This material is available free of charge via the Internet at <http://pubs.acs.org>.

JA0362196

(66) Pantelides, S. T.; DiVentra, M.; Lang, N. D. *Physica B* **2001**, 296, 72.

(67) DiVentra, M.; Pantelides, S. T.; Lang, N. D. *Phys. Rev. Lett.* **2000**, 84, 979.

(68) Crispin, X.; Geskin, V. M.; Bureau, C.; Lazzaroni, R.; Schmickler, W.; Bredas, J. L. *J. Chem. Phys.* **2001**, 115, 10493.

(69) Mazur, U.; Hipps, K. W. *J. Phys. Chem.* **1994**, 98, 8169.

(70) Segal, D.; Nitzan, A.; Ratner, M.; Davis, W. D. *J. Phys. Chem. B* **2000**, 104, 2790.

(71) Burin, A. L.; Ratner, M. A. *J. Phys. Chem.* **2000**, 113, 3941.